Time Reversal With the FDTD Method for Microwave Breast Cancer Detection

Panagiotis Kosmas, *Member, IEEE,* and Carey M. Rappaport, *Senior Member, IEEE*

***Abstract*—The feasibility of microwave breast cancer detection with a time-reversal (TR) algorithm is examined. This algorithm is based on the finite-difference time-domain method, and compensates for the wave decay and, therefore, is suitable for lossy media. In this paper, we consider a two-dimensional breast model based on magnetic resonance imaging data, and examine the focusing abilities of a TR mirror comprised of an array of receivers with a single ultra-wideband pulse excitation. In order to resolve small 3-mm-diameter tumors, a very short duration pulse is necessary, and this requirement may restrict the applicability of the system due to hardware limitations. We propose a way to overcome this obstacle based on the observation that the amplitude and phase information of the tumor response is sufficient to achieve focusing. The robustness of the TR algorithm with respect to breast inhomogeneities is demonstrated, and the good performance of the method suggests it is a promising technique for microwave breast cancer detection.**

***Index Terms*—Finite difference time domain (FDTD), microwave imaging, time reversal (TR).**

I. Introduction

MOTIVATED by data [1]–[4], which reveal an important contrast in the electromagnetic properties of malignant tumor tissue relative to normal fatty breast tissue, several microwave imaging techniques for breast cancer detection have been recently developed. Encouraging results have been obtained with near-field tomographic image reconstruction algorithms [5], [6], confocal microwave imaging (CMI) techniques [7], and microwave imaging based on space-time (MIST) beamforming [8]. Meaney *et al.* have presented results with simulation and phantom data, as well as some preliminary clinical exams [9], and experimental results using phantom data have also been reported for the cylindrical CMI system [10] and the MIST planar system [11].

This paper examines the possibility of tumor detection and localization using the principles of time reversal (TR). In acoustics, physical TR experiments using transducers, which time reverse the received signal and re-emit it through the medium, have shown that the time-reversed wave focuses back to the source target in the presence of an inhomogeneous lossless medium [12]. Recently, the first attempt to perform an electromagnetic TR experiment was also reported [13]. Aside from physical experiments, a virtual procedure similar to a physical TR can be used for microwave imaging purposes. This backpropagation technique can be performed directly in the time domain using the finite-difference time-domain (FDTD) method [14]. The use of the FDTD method for TR purposes has been a topic of interest in geophysical applications, where it is more commonly described as time migration [15]. In addition, the FDTD method has been applied to calculate the adjoint backpropagation operation in simple inverse scattering schemes [16].

The possibility of time-reversing the FDTD equations was presented in [17]. There it was shown that if a point source radiates in free space and the time-reversed FDTD equations are applied to all points of the grid, the wave will converge back to the source at time corresponding to the maximum of the initial excitation. TR algorithms based on the transmission-line method (TLM) have also been proposed [18]. In this paper, we present an FDTD TR algorithm that compensates for the medium's ohmic losses and is, therefore, equally applicable to lossless and lossy media. The key properties of the algorithm are illustrated with a simulation of an inverse source-type problem [19] in Section II. In Section III, we apply this technique to detect and localize malignant tumor-like anomalies in the breast, based on the target response received by an array of antennas, when one single point source is used for transmission. In previous study, the FDTD TR algorithm was tested for tumor detection in a semiellipsoidal homogenous two-dimensional (2-D) breast model [20]. In this paper, a realistic breast model based on magnetic resonance imaging (MRI) data is used. We consider a 2-D slice of the breast and include a skin layer and inhomogeneities in the breast tissue, which is assumed to be nondispersive. Previous simulations in [20] have shown that the FDTD TR model is, in general, robust to dispersion and measurement noise and, therefore, these aspects of the problem are not examined here.

The main goal of this paper is to show that focusing can be achieved even when certain properties of the background medium are not known *a priori*, as will be the case in a realistic microwave breast cancer detection application. In particular, it is shown that omitting the skin layer and the distribution of the breast inhomogeneities from the breast model in the TR process does not affect the focusing of the wave back to the target. Finally, in Section IV, we conclude with a discussion on the future

Manuscript received July 28, 2004; revised February 27, 2005. This work was supported by the Center for Subsurface Sensing and Imaging Systems, Northeastern University, under the Engineering Research Centers Program of the National Science Foundation Award EEC-9986821.

P. Kosmas was with the Center for Subsurface Sensing and Imaging Systems, Northeastern University, Boston, MA USA 02115. He is now with the Wireless Communications Research Group, Loughborough University, Loughborough LE11 3TU, U.K.

C. M. Rapapport is with the Center for Subsurface Sensing and Imaging Systems, Northeastern University, Boston, MA 02115 USA (e-mail:pkosmas@coe.neu.edu).

Digital Object Identifier 10.1109/TMTT.2005.850444

extension of this study and an overview of the aspects of this approach in relation to other methods, which have been proposed in the literature.

II. Electromagnetic TR With the FDTD Method

The derivation of the time-reversed FDTD equations is straightforward, taking into account that under the TR transformation $t' = -t$, the following equalities are true [21].

- $\rho(t') = \rho(t)$.
- $\mathbf{E}(\mathbf{t}') = \mathbf{E}(\mathbf{t})$.
- $\mathbf{B}(\mathbf{t}') = -\mathbf{B}(\mathbf{t})$.
- $\mathbf{J}(\mathbf{t}') = -\mathbf{J}(\mathbf{t})$.

To illustrate the method, we write the TR equations for the 2-D TM_x case in a lossy medium. Following the standard FDTD notation, we have

$$\begin{aligned} E_x^{n'+1/2}(j,k) &= E_x^{n'-1/2}(j,k) \\ &\quad - \frac{\Delta t}{\varepsilon \Delta}\Bigg\{ H_z^{n'}\left(\frac{j+1}{2},k\right) - H_z^{n'}\left(\frac{j-1}{2},k\right) \\ &\qquad - H_y^{n'}\left(j,\frac{k+1}{2}\right) + H_y^{n'}\left(j,\frac{k-1}{2}\right) \\ &\qquad + \sigma \Delta E_x^{n'+1/2}(j,k)\Bigg\} \end{aligned} \tag{1}$$

$$\begin{aligned} H_y^{n'+1}\left(j,\frac{k+1}{2}\right) &= H_y^{n'}\left(j,\frac{k+1}{2}\right) + \frac{\Delta t}{\mu \Delta} \\ &\quad \times \left\{ E_x^{n'+1/2}(j,k+1) - E_x^{n'+1/2}(j,k)\right\} \end{aligned} \tag{2}$$

$$\begin{aligned} H_z^{n'+1}\left(\frac{j+1}{2},k\right) &= H_z^{n'}\left(\frac{j+1}{2},k\right) - \frac{\Delta t}{\mu \Delta} \\ &\quad \times \left\{ E_x^{n'+1/2}(j+1,k) - E_x^{n'+1/2}(j,k)\right\} \end{aligned} \tag{3}$$

where $\Delta x = \Delta y = \Delta$ is the grid spacing and Δt is the temporal increment. The $(n' + 1/2)$ time step corresponds to the next step of the backpropagated equations, which is the previous time step in relation to the real time sequence. Thus, while n' and Δt denote the iteration step and temporal increment of the FDTD algorithm and, therefore, have positive values, the temporal evolution of the computational TR algorithm is expressed as $t = T - n'\Delta t$, where T is the initial time when backpropagation begins.

It is important to note that (1)–(3) imply a TR system where the propagating medium is reversed and, thus, losses are compensated, as it is clearly seen from the change of sign in the conductivity in (1). Such a system differs from physical TR or traditional numerical backpropagation [22], where the time-reversed wave is propagated into the same medium. As an example of this approach, we consider an ideal experiment, which corresponds to the concept of a time reversal cavity (TRC), first introduced and analyzed in [23]. For the 2-D TM_z case that we consider, a TRC assumes that the electric field is available for all points at the four sides of a rectangular surface, which surrounds the source. To simulate the experiment, we excite a point source with a modulated Gaussian pulse of 2-GHz center frequency and let the fields propagate in the FDTD grid of size 249 $\Delta\times$ 249 Δ. We record the electric field on the four sides of a square of side 50 Δ, and stop the forward simulations at time $N\Delta t$, with N being the number of iterations and Δt being the time step. We then time reverse the recorded waveforms, and run the model described by (1)–(3) for a maximum amount of N time steps.

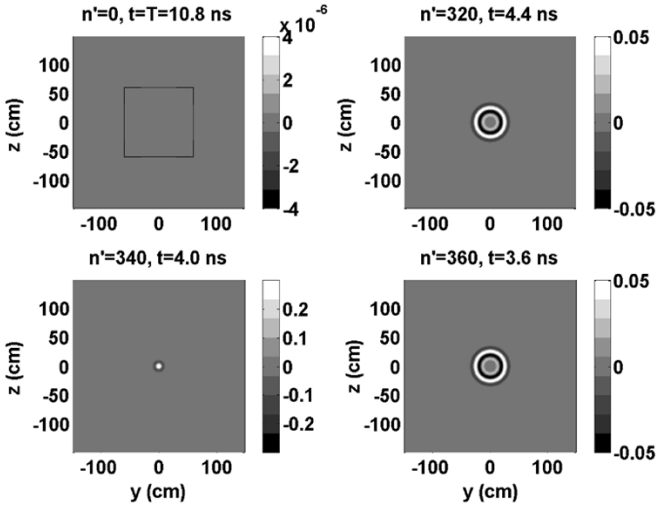

Fig. 1. Progression of the time-reversed electric field as function of time. Backpropagation starts at $t = T$, and the wave gradually converges ($t = T - 6.4$ ns) to its origin at optimal time $t = T - 6.8$ ns, and then diverges again ($t = T - 7.2$ ns) with the diverging wave being an exact time-reversed replica of the converging wave.

An example of this procedure is given in Fig. 1, where a sequence of "snapshots" of the electric-field distribution is shown on the yz-plane. The time step of these simulations is $\Delta t = 20$ ps and the cell size is $\Delta = 1.2$ cm. The short duration pulse has a width of $W = 16\ \Delta t$ with its peak occurring at $T_0 = 200\ \Delta t$. The top left-hand-side figure shows the fields at the initial time T for the time-reversed model, which are nonzero only for the four sides where they are recorded, at 50 Δ, while the rest of the "snapshots" show the temporal evolution of the computational TR simulations.

This figure can be easily interpreted based on TR theory; it is actually an illustration of the theoretical analysis given in [23]. Similar to [23], we can write the electric-field distribution as

$$E_x(\mathbf{r},t) = \phi(T-t) \otimes K(\mathbf{r},t) \tag{4}$$

where $\otimes$ denotes temporal convolution and

$$K(\mathbf{r},t) = \frac{1}{4\pi\mathbf{r}}\delta\left(t + \frac{|\mathbf{r}|}{c}\right) - \frac{1}{4\pi\mathbf{r}}\delta\left(t - \frac{|\mathbf{r}|}{c}\right). \tag{5}$$

Equations (4) and (5) imply that the time-reversed field depends on the excitation waveform $\phi(t)$ and a kernel distribution, which is the difference of a converging and diverging wave, with an arrival time difference equal to $2|\mathbf{r}|/c$. For a short-duration pulse,

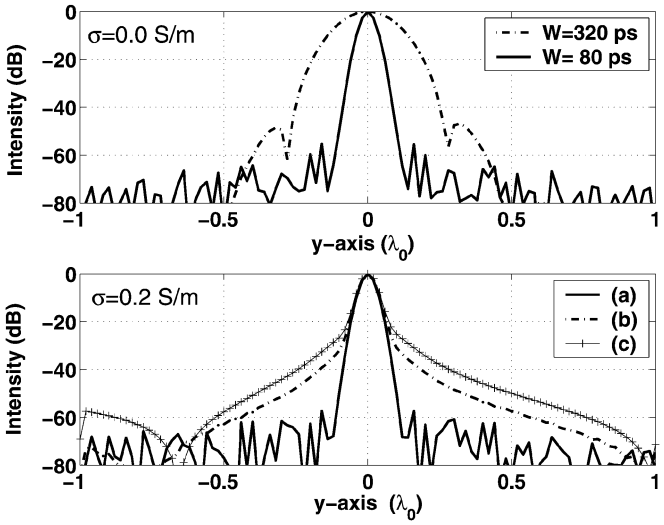

Fig. 2. Intensity patterns (cross-range) as function of central wavelength for the inverse source problem in a lossless and lossy dielectric ($\varepsilon_r = 2.9$). In the top figure, the field intensity is plotted for two pulses of different width. Focusing for a lossy medium of $\sigma = 0.2$ S/m (bottom) is similar when the medium is time-reversed (a), but deteriorates if the losses are ignored (b), or the (back)propagating lossy medium remains unchanged (c).

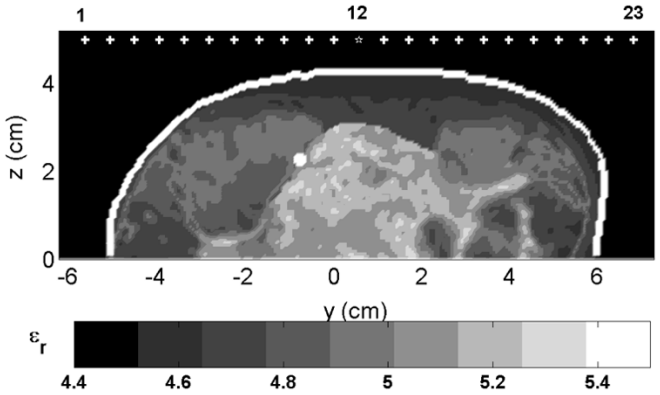

Fig. 3. 2-D MRI-based breast model for the 2-D FDTD grid used to generate the data for input to the TR system. Element #12 of the TRM is also the transmitter of the system. The skin layer and 3-mm-diameter tumor-like spherical scatterer are artificially introduced.

the two waveforms can be separated in time. This is clearly observed in Fig. 1; the converging wave first focuses at the source and the diverging wave follows and occurs as a time-reversed replica of the converging wave. The optimum focusing occurs at $(T - 6.8)$ ns, which naturally corresponds to the peak time T_0. For a very short temporal duration pulse, there is no significant interference between the converging and diverging wave, and the resolution of the system depends on the smallest significant wavelength of the pulse. Thus, short temporal duration pulses will lead to a much higher resolution than a monochromatic excitation.

We now turn our attention to an important aspect of the time-reversed FDTD equations, the loss compensation via the sign change of the conductivity in (1). Being able to retrieve attenuated waves, FDTD TR can be applied to lossy media leading to focusing quality identical to the one achieved in the lossless case. This important property of the system is shown in Fig. 2. The propagating medium now is a hypothetical lossy dielectric with dielectric constant $\varepsilon_r = 2.9$ and conductivity $\sigma = 0.2$ S/m. This relatively high ratio of σ to ε_r was chosen in order to study the effect of inverting the conductivity sign in the time-reversed equations. Case (a) of the bottom plot employs this change in the conductivity, leading to results identical to the lossless case, shown in the top plot for comparison. We have also considered a TR system, which assumes no loss for the propagating medium (b) and one which time reverses the fields, but does not change the medium (c). It is evident from this figure that, although the resolution stays the same until -20 dB, there is focusing degradation for cases (b) and (c), which is observed in the 2-D images as sidelobes around the source, and only case (a) can recover the fields, as well as the lossless case. The top plot also illustrates the resolution dependence on the pulsewidth, implying that the choice of using ultra-wideband excitation pulses is necessary in order to achieve the desirable resolution. Finally, we should also note that this loss compensation is only possible for moderately conductive media, where displacement currents are dominant. In the case of a strongly conducting medium, the reversed time Cauchy problem is ill posed and unstable [24].

III. Application to Tumor Detection

A. FDTD Model and System Configuration

The general properties of the system observed for the inverse source problem will equally apply to the inverse-scattering problem when treated in the context of the (distorted wave) Born approximation (DWBA) [25]. While the DWBA assumes that the background medium is known, in a real application, some of the medium's properties such as breast inhomogeneities and skin thickness are not available and may have to be estimated. The simulations presented here will show that the time-reversed scattered field focuses back to the tumor even when an approximation of the background medium is used, which does not require knowledge of the properties in question.

The geometry that generates synthetic data for our reconstructions is shown in Fig. 3. The proposed TR system is comprised of an array of 23 receivers located at a small distance from the top of the breast, with the middle also acting as a transmitter of a differentiated Gaussian pulse of 50-ps width. This source location ensures that reflections from the chest wall do not obscure detection for tumors that are not close to the chest wall [26]. In this initial investigation, specific antenna elements are not modeled and, therefore, a receiver element represents an observation point, and the transmitter is a point source assigned an electric field E_x (TM configuration). The various tissues are considered nondispersive with values of permittivity and conductivity taken from dispersive models that fit published data [4]. Although modeling dispersion is important for an accurate prediction of the system response [26], time reversing the dispersive medium is nontrivial and, therefore, we choose to omit dispersion in our forward models. Our results are expected to apply, in general, to the dispersive case.

Based on the MRI data, the regions corresponding to fibroglandular regions in the breast were linearly mapped to higher permittivity and conductivity values with an upper bound of 16% of the nominal values for breast fat, which are set at $\varepsilon_r =$

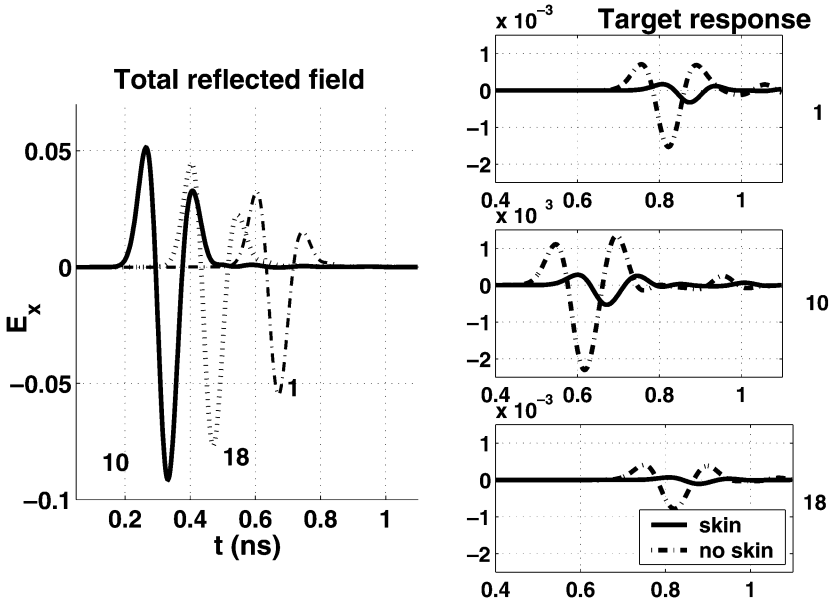

Fig. 4. Normalized reflected (left-hand side) and scattered from the tumor (right-hand side) electric field at three of the receivers of the system. The presence of skin only introduces additional scaling and delay to the tumor signal compared to an idealized case of no skin.

4.58 and $\sigma = 0.52$ S/m. The resulting permittivity values for the various regions are shown in this figure. In addition, a skin layer ($\varepsilon_r = 31$, $\sigma = 5.8$ S/m) of thickness varying with position from 1.5 to 2 mm, and a spherical (3-mm diameter) tumor-like scatterer ($\varepsilon_r = 39$, $\sigma = 8$ S/m) are artificially introduced as shown in this figure. The surrounding medium is a lossless dielectric with dielectric constant $\varepsilon_r = 4.48$, which closely matches the nominal value of breast fat.

Samples of the electric field scattered from the tumor, as observed in three of the receivers, are shown in Fig. 4. This field is obtained by subtracting the fields calculated from a model with and without the tumor. Also plotted for comparison is the response at each receiver after removal of the field due to the transmitter, which can be obtained by a simulation in the absence of the breast. This response is dominated by skin reflections, and also includes clutter due to inhomogeneities and reflections from the chest wall. A close observation of the signals in this figure shows that the tumor acts as a point scatterer, which only introduces an amplitude scaling and a time delay to the shape of the total reflected field. The point scatterer assumption suggests that multiple scattering can be ignored and TR is suitable for imaging. In Section III-B, we discuss some implementation aspects of the application of the FDTD TR algorithm to tumor detection, and present simulations, which show that the TR model does not require information on the skin properties or the distribution of the breast inhomogeneities.

B. TR Imaging

An important aspect of computational TR, performed directly in the time domain for imaging, is choosing the optimal time instant when the wave focuses back to the scatterer. This instant depends on the location of the scatterer and, therefore, cannot be known *a priori*. To understand the importance of determining the optimal time instant for successful localization of the target, one can look back at the illustration of the inverse source problem presented in Fig. 1. As the TR procedure progresses, the converging wave is followed by a wave that diverges away from the source, and focusing is achieved for the very small time interval in between these two interfering waves. In this ideal case, where all data are available and the background medium is known, the time-reversed field reaches its peak at the optimal time instant when it focuses back to the source. This is due to the spatio-temporal matched filtering achieved by the TR process [12]. However, in an application where only an array of receivers is used and uncertainties about the background medium are inevitable, this criterion may lead to a false image, and an additional criterion should also be sought.

When the wave focuses back to the source scatterer, it is expected to produce an image with a sharp peak at the target location and small structure elsewhere. Since such images have small entropy, a minimum entropy criterion can be employed for the choice of the optimal image and the corresponding time instant. To compute the entropy, we calculate the inverse varimax norm, which has been previously employed in numerical backpropagation applications for land-mine detection [27]. Given that the electric field is available everywhere and for every time step in the FDTD TR model, we calculate the quantity

$$R(E_x^n) = \frac{\left[\sum\sum\limits_{j,k} E_x^{n2}(j,k)\right]^2}{\sum\sum\limits_{j,k} E_x^{n4}(j,k)} \tag{6}$$

where n is the time step of the FDTD TR algorithm, (j,k) are the grid cell coordinates, and summation is over the portion of the grid that represents the breast. The fields at the time instant where the varimax norm (6) is minimized are stored as the output of the FDTD TR algorithm. The minimum entropy criterion is quite robust with respect to the input signal. Plots of the entropy as function of time show a monotonically decreasing

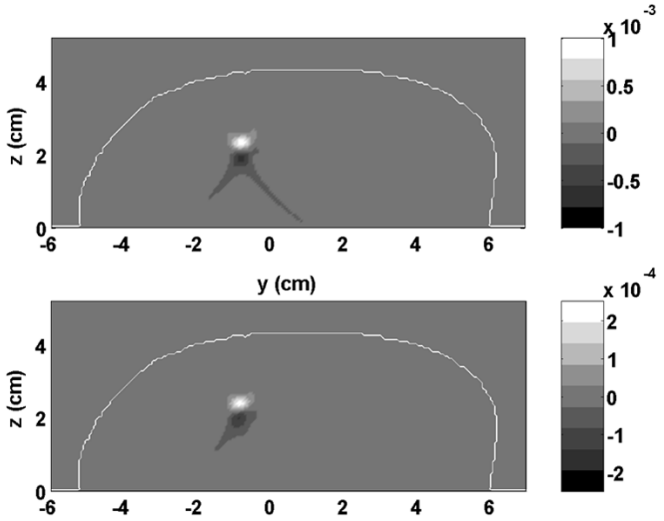

Fig. 5. Time-reversed electric field for the breast model of Fig. 3 when skin is not considered (top) and when the skin layer is introduced (bottom). The breast in both cases is considered homogeneous, and the skin effect in the bottom case is perfectly removed.

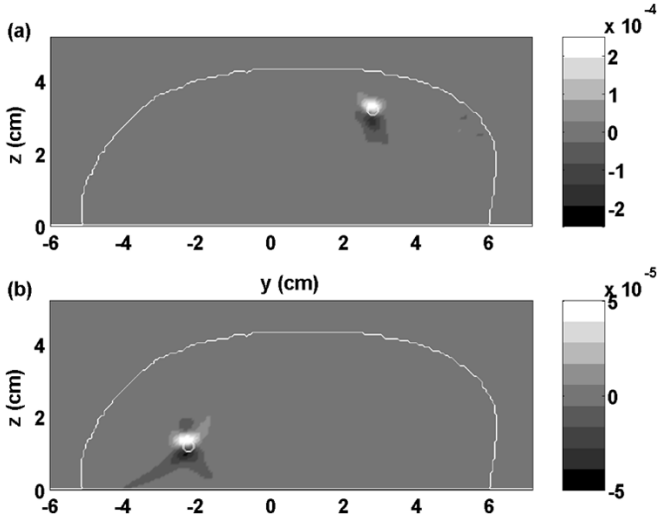

Fig. 6. Same as in Fig. 5 for two additional tumor locations, marked with white circles.

curve, which reaches a distinct minimum, before it starts to increase again to its higher initial values. Small errors in localization may occur since the criterion guarantees a tightly focused image, but not the maximum power at the focus.

As it was shown in Section III-A, resolution depends on the temporal width of the exciting signal. In order to resolve tumors of diameter, which is only a fraction of the wavelength corresponding to the central frequency of the excitation signal, ultrawideband signals of very high-frequency content need to be used. This requirement can impose a restriction, which cannot be realized in practice due to hardware limitations. Thus, in order to achieve focusing with high resolution independently of the transmitted pulse, we backpropagate a temporally windowed version of the target signal, by multiplying its response with a very short Gaussian pulse centered at its peak. The input signal for backpropagation at each receiver can be expressed as

$$g_i(t) = E_x(y_i, z_i) \cdot e^{-((t-tp)/\tau)^2} \tag{7}$$

where t_p is the time instant where the peak of the received waveform $E_x(y_i, z_i)$ occurs, and τ is the taper parameter, which determines the width of the impulse temporal function. The input functions g_i maintain the necessary amplitude-phase information, and their use enables focusing with very high resolution, as will be shown from the below simulations. A similar concept has recently been explored in ultrasonic applications of iterative TR for the detection of multiple targets [28].

Our primary goal is to examine what information on the background medium is essential for the TR algorithm to focus back to the tumor-like scatterer. This information can be used in two ways: first, to remove the clutter from the total signal and, therefore, obtain the true signal scattered from the target and, second, to construct the medium that will be used in the TR algorithm. Our simulations show that while backpropagating the true target response is essential, knowledge of the inhomogeneities or the skin thickness for the TR model is not necessary. An example of this important property of the system is shown in Fig. 5. Here, we time reverse the exact field scattered from the tumor in Fig. 3 by using the temporal windowing approach described above. The TR model considers a homogeneous breast filled with an average value of ε_r and σ, and no skin. In plot (a), we time-reverse data from the breast model without the skin, while in (b) the skin layer is introduced. Additional results of this second case with the skin for two more locations, one closer to the skin and one in the proximity of the chest wall, are shown in Fig. 6.

It is clear from these figures that focusing is achieved in all cases. The focused wave features a (white) region of maximum field intensity, which should be identified as the area where the target is located, followed by a region of negative field intensity, which is an artifact due to the limited data configuration. For an appropriate choice of the parameter τ in (7), the size of the region of focus in Figs. 5 and 6 is comparable to the physical size of the tumor, and the location of the focus is very close to the true location of the target. For example, the area of focus for the two first locations in Figs. 5 and 6 is a square of approximate size 9 mm^2, which is very close to the physical size of the target, and the square's center is at the top of the target. For the third location, the focal area is slightly greater, and the localization is slightly worse, but still quite accurate.

Since focusing depends upon the ability to identify the tumor response from the total signal at each receiver, any algorithm that removes the clutter due to inhomogeneities and skin reflections can be used prior to TR of the resulting scattered field. For example, an algorithm that removes the skin-breast artifact was presented in [8]. Successful removal of the clutter depends upon the degree of correlation between the tumor and the dominant skin response. This very important aspect of the problem will be treated in detail in future work. Here, we examine a simple approach, which aims to detect the tumor in the presence of the unknown inhomogeneities and can be readily applied to the total field data, but assumes the skin response can be perfectly removed. For each receiver, the signal from a simulation that considers homogeneous breast fat and skin, but no tumor, is subtracted from the total field. The resulting signal is due to the tumor-like target and the breast inhomogeneities.

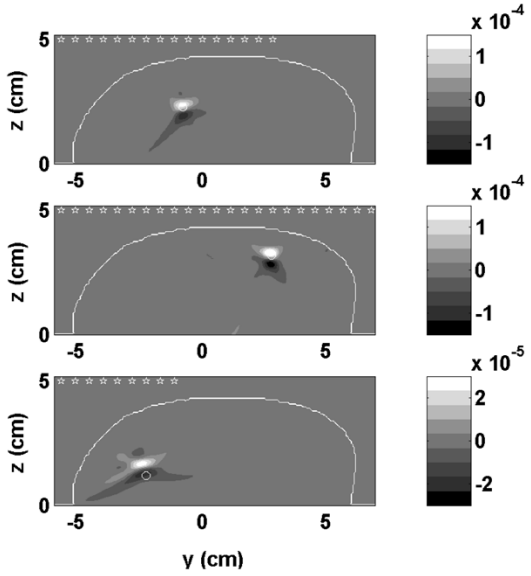

Fig. 7. Time-reversed electric field for three different 3-mm-diameter tumor locations for an inhomogeneous breast model. The received field is backpropagated after perfect removal of the skin reflections (assumed to be known *a priori*, and a simple algorithm for averaging the effect of the breast *a priori*). The receivers used in the TR procedure are marked with stars.

To remove the background signal, we align and scale each signal, calculate the average, and subtract it from each receiver after appropriate realignment and scaling. The results for the three different target locations are shown in Fig. 7. For each case, the receivers that are used in the TR procedure are marked with a star. The signal at those receivers can be clearly identified as due to the presence of a target, while for the remaining receivers, the clutter is still comparable to the target contributions after the simple averaging procedure is applied. These latter receivers are omitted from the TR process. As it is seen from this figure, the system is able to resolve the small tumor and localize it accurately, with a small error in the third case, since the suggested TR mirror (TRM) is more suitable for tumors that are not buried too deep in the breast. For this third case, the signal due to the tumor after the clutter removal algorithm can be identified for a smaller number of receivers and, therefore, focusing quality is deteriorated. A more sophisticated algorithm that would identify the tumor signal more accurately is expected to produce better performance for our imaging system. Such an algorithm will be presented in future study.

IV. Summary and Conclusions

This paper has presented a new approach to microwave breast cancer detection based on numerical TR with the FDTD method. The featured FDTD TR algorithm compensates for the medium's losses and is, therefore, applicable to lossy media. For a 3-mm-diameter tumor-like target in a breast model based on MRI data, it was shown that an array of receivers can resolve the target with high resolution by using a temporally windowed version of the target response as the input in the TR process. An important aspect of this study is the separation of the tumor detection problem into two independent processes; the first aims to estimate the scattered field form the tumor as accurately as possible using detection techniques, while the second time reverses this field using the presented TR model. The second process is robust to uncertainties in the medium and, thus, the overall performance depends on the first step, i.e., the successful identification of the tumor response from the total signal at each receiver. A simplified example of combining these two steps was given, leading to successful detection and localization of the tumor.

In a future paper, an algorithm that identifies the tumor signal to be used in the first step of our TR imaging algorithm will be presented. Other important aspects of the problem, such as false alarms, will also be investigated. The preliminary results presented here, however, encourage us to believe that the method is a promising technique for microwave breast cancer detection. Among its advantages, one should note its simplicity in implementation, and its ability to accurately model complex background media. TR has been shown to be superior to other simple delay-based focusing techniques, especially in inhomogeneous media [12]. The additional feature of our algorithm to compensate for losses is also an advantage over techniques such as CMI, where the compensation step is performed only approximately. The FDTD TR algorithm also has the potential to account for dispersion effects, and is relatively fast; the 2-D versions presented here take about 1 min of execution time on a Pentium III PC. The robustness of the method with respect to the medium's uncertainties is another very desirable feature. On the other hand, the technique is very sensitive to the ability of the system to identify the target signal from clutter. In addition, it assumes a linearization in the inverse-scattering problem, and does not provide any information on the shape or the actual size of the tumor, but only localizes its origin. A more complete future analysis of the application of this approach to a more realistic breast cancer detection problem will shed light onto some of the aspects of the method discussed here.

Acknowledgment

The authors would like to thank Dr. M. Doyley, Darthmouth Medical School, Hanover, NH, for providing the MRI breast data. Author P. Kosmas would like to thank Prof. E. Miller and Prof. A. Devaney, both of Northeastern University, Boston, MA, for helpful discussions on various components of this study.

References

[1] W. T. Joines, Y. Z. Dhenxing, and R. L. Jirtle, "The measured electrical properties of normal and malignant human tissues from 50 to 900 MHz," *Med. Phys.*, vol. 21, pp. 547–550, Apr. 1994.

[2] S. S. Chaudhary, R. K. Mishra, A. Swarup, and J. M. Thomas, "Dielectric properties of normal and malignant human breast tissues at radiowave and microwave frequencies," *Indian. J. Biochem. Biophys.*, vol. 21, pp. 76–79, Feb. 1984.

[3] C. Gabriel, S. Gabriel, and E. Corthout, "The dielectric properties of biological tissues: I. Literature survey," *Phys. Med. Biol.*, vol. 41, pp. 2231–2249, Nov. 1996.

[4] S. Gabriel, R. W. Lau, and C. Gabriel, "The dielectric properties of biological tissues: II. Measurements on the frequency range 10 Hz to 20 GHz," *Phys. Med. Biol.*, vol. 41, pp. 2251–2269, Nov. 1996.

[5] D. Li, P. M. Meaney, and K. D. Paulsen, "Confocal microwave imaging for breast cancer detection," *IEEE Trans. Microw. Theory Tech.*, vol. 51, no. 4, pp. 1179–1186, Apr. 2003.

[6] A. E. Bulyshev, S. Y. Semenov, A. E. Souvorov, R. H. Svenson, A. G. Nazarov, Y. E. Sizov, and G. P. Tatsis, "Computational modeling of three-dimensional microwave tomography of breast cancer," *IEEE Trans. Biomed. Eng.*, vol. 48, no. 9, pp. 1053–1056, Sep. 2001.

[7] E. C. Fear, X. Li, S. C. Hagness, and M. A. Stuchly, "Confocal microwave imaging for breast tumor detection: Localization in three dimensions," *IEEE. Trans. Biomed. Eng.*, vol. 49, no. 8, pp. 812–822, Aug. 2002.
[8] E. J. Bond, X. Li, S. C. Hagness, and B. D. Van Veen, "Microwave imaging via space-time beamforming for early detection of breast cancer," *IEEE Trans. Antennas Propag.*, vol. 51, no. 8, pp. 1690–1705, Aug. 2003.
[9] P. M. Meaney, M. W. Fanning, D. Li, S. P. Poplack, and K. D. Paulsen, "A clinical prototype for active microwave imaging of the breast," *IEEE Trans. Microw. Theory Tech.*, vol. 48, no. 11, pp. 1841–1853, Nov. 2000.
[10] E. C. Fear, J. Sill, and M. A. Stuchly, "Experimental feasibility study of confocal microwave imaging for breast tumor detection," *IEEE Trans. Microw. Theory Tech.*, vol. 51, no. 3, pp. 887–892, Mar. 2003.
[11] X. Li, S. C. Hagness, B. D. Van Veen, and D. Van der Weide, "Experimental investigation of microwave imaging via space-time beamforming for breast cancer detection," in *IEEE MTT-S Int. Microwave Symp. Dig.*, Jun. 2003, pp. 379–382.
[12] M. Fink, D. Cassereau, A. Derode, C. Prada, P. Roux, M. Tanter, J. L. Thomas, and F. Wu, "Time-reversed acoustics," *Rep. Prog. Phys.*, vol. 63, pp. 1933–1995, 2000.
[13] G. Lerosey, J. de Rosny, A. Tourin, A. Derode, G. Montaldo, and M. Fink, "Time reversal of electromagnetic waves," *Phys. Rev. Lett.*, vol. 92, pp. 1 939 041–1 939 043, May 2004.
[14] A. Taflove and S. C. Hagness, *Computational Electrodynamics: The Finite-Difference Time-Domain Method*. Boston, MA: Artech House, 2000.
[15] C. J. Leuschen and R. G. Plumb, "A matched-filter-based reverse-time migration algorithm for ground-penetrating radar data," *IEEE Trans. Geosci. Remote Sens.*, vol. 39, no. 5, pp. 929–936, May 2001.
[16] T. Tanaka, T. Takenaka, and S. He, "An FDTD approach to the time-domain inverse scattering problem for an inhomogeneous cylindrical object," *Microwave Opt. Technol. Lett.*, vol. 20, pp. 72–77, Jan. 1999.
[17] R. Sorrentino, L. Rosseli, and P. Mezzanote, "Time-reversal in finite difference time domain method," *IEEE Microw. Guided Wave Lett.*, vol. 3–11, no. 11, pp. 402–404, Nov. 1993.
[18] M. Forest and W. J. R. Hoefer, "TLM synthesis of microwave structures using time reversal," in *IEEE MTT-S Int. Microwave Symp. Dig.*, Jun. 1992, pp. 779–782.
[19] E. A. Marengo and A. J. Devaney, "The inverse source problem in the time domain," in *IEEE AP-S Symp.*, Jun. 1998, pp. 21–26.
[20] P. Kosmas and C. Rappaport, "Use of the FDTD method for time reversal: Application to microwave breast cancer detection," in *Proc. SPIE Computer Imaging*, vol. 5299, San Jose, CA, Jan. 2004, pp. 1–9.
[21] C. Altman and K. Suchy, *Reciprocity, Spatial Mapping and Time Reversal in Electromagnetics*. Amsterdam, The Netherlands: Kluwer, 1991.
[22] A. J. Devaney, "Super-resolution processing of multistatic data using time reversal and music," , 1999 (preprint).
[23] D. Cassereau and M. Fink, "Time reversal of ultrasonic fields—Part III: Theory of the closed time-reversal cavity," *IEEE Trans. Ultrason., Ferroelectr., Freq. Control*, vol. 39, no. 5, pp. 579–592, Sep. 1992.
[24] M. V. Klibanov and A. Timonov, "On the mathematical treatment of time reversal," *Inv. Prob.*, vol. 19, pp. 1299–1318, Oct. 2003.
[25] A. J. Devaney and M. Oristaglio, "Inversion procedure for inverse scattering within the distorted wave born approximation," *Phys. Rev. Lett.*, vol. 51, pp. 237–240, Jul. 1983.
[26] P. Kosmas and C. Rappaport, "Modeling with the FDTD method for microwave breast cancer detection," *IEEE Trans. Microw. Theory Tech.*, vol. 52, no. 8, pp. 1890–1897, Aug. 2004.
[27] X. Xu, E. L. Miller, and C. M. Rappaport, "Minimum entropy regularization in frequency-wavenumber migration to localize subsurface objects," *IEEE Trans. Geosci. Remote Sens.*, vol. 41, no. 8, pp. 1804–1812, Aug. 2003.
[28] G. Montaldo, M. Tanter, and M. Fink, "Real time inverse filter focusing through iterative time reversal," *J. Acoust. Soc. Amer.*, vol. 115, no. 2, pp. 768–775, Feb. 2004.

Panagiotis Kosmas (S'03–M'05) received the Diploma degree in electrical and computer engineering from the National Technical University of Athens, Athens, Greece in 1999, and the M.S. and Ph.D. degrees in electrical engineering from Northeastern University, Boston, MA, in 2002 and 2005, respectively.

From January 2000 to February 2005, he was a Research Assistant with the Department of Electrical Engineering and the Center for Subsurface Sensing and Imaging Systems, Northeastern University. Since April 2005, he has been a Post-Doctoral Research Associate with the Wireless Communications Research Group, Loughborough University, Loughborough, U.K. His research interests include computational electromagnetics, and the finite-difference time-domain method in particular, antenna modeling and design, as well as inverse problems and signal-processing techniques.

Carey M. Rappaport (S'80–M'87–SM'96) received the S.B. degree in mathematics, the S.B., S.M., and E.E. degrees in electrical engineering, and the Ph.D. degree in electrical engineering from the Massachusetts Institute of Technology (MIT), Cambridge, in 1982, 1982, 1982, 1982, and 1987, respectively.

From 1981 to 1987, he was a Teaching and Research Assistant with MIT. During the summers from 1981 to 1987, he was with COMSAT Laboratories, Clarksburg, MD, and The Aerospace Corporation, El Segundo, CA. In 1987, he joined the faculty of Northeastern University, Boston, MA, where, since July 2000, he has been a Professor of electrical and computer engineering. During Fall 1995, he was a Visiting Professor of electrical engineering with the Electromagnetics Institute, Technical University of Denmark, Lyngby, Denmark, as part of the W. Fulbright International Scholar Program. He has consulted for Geo-Centers Inc., PPG Inc., and several municipalities on wave propagation and modeling, and microwave heating and safety. He was Principal Investigator of an Army Research Office (ARO)-sponsored Multidisciplinary University Research Initiative on Demining and Co-Principal Investigator of the National Science Foundation (NSF)-sponsored Center for Subsurface Sensing and Imaging Systems (CenSSIS) Engineering Research Center. He has authored over 200 technical journal and conference papers in the areas of microwave antenna design, electromagnetic-wave propagation and scattering computation, and bioelectromagnetics. He holds two reflector antenna patents, two biomedical device patents, and three subsurface sensing device patents.

Prof. Rappaport is a member of Sigma Xi and Eta Kappa Nu. He was the recipient of the1986 IEEE Antenna and Propagation Society (AP-S) H. A. Wheeler Award for the best applications paper as a student.